Nanotechnology **18** (2007) 415302 (6pp) doi:10.1088/0957-4484/18/41/415302

Self-assembly and optical properties of patterned ZnO nanodot arrays

Yijian Song[1], **Maojun Zheng**[1,3] **and Li Ma**[2]

[1] Laboratory of Condensed Matter Spectroscopy and Opto-Electronic Physics, Department of Physics, Shanghai Jiao Tong University, Shanghai 200240, People's Republic of China
[2] School of Chemistry and Chemical Technology, Shanghai Jiao Tong University, Shanghai 200240, People's Republic of China

E-mail: mjzheng@sjtu.edu.cn

Received 11 June 2007, in final form 22 August 2007
Published 12 September 2007
Online at stacks.iop.org/Nano/18/415302

Abstract
Patterned ZnO nanodot (ND) arrays and a ND-cavity microstructure were realized on an anodic alumina membrane (AAM) surface through a spin-coating sol–gel process, which benefits from the morphology and localized negative charge surface of AAM as well as the optimized sol concentration. The growth mechanism is believed to be a self-assembly process. This provides a simple approach to fabricate semiconductor quantum dot (QD) arrays and a QD-cavity system with its advantage in low cost and mass production. Strong ultra-violet emission, a multi-phonon process, and its special structure-related properties were observed in the patterned ZnO ND arrays.

(Some figures in this article are in colour only in the electronic version)

1. Introduction

ZnO is a wide-band-gap semiconductor with large exciton energy and excellent thermal and chemical stability, which makes its nanomaterial have great potential in applications in ultraviolet lasers, solar cells, gas sensors, bio-detectors [1–4], etc. Various kinds of ZnO nanostructures, such as spherical nanoparticles, nanorods, helical nanorods, nanoplates, nanowalls, nanotriangles, nanobelts, nanorings, hexagonal disks, tetrapods, etc, have already been successfully synthesized through different approaches including thermal evaporation, the vapor transport process, electron-beam evaporation, the sol–gel technique, and hydrothermal synthesis [5–18]. Recently, the growth of a ZnO nanostructure via a wet-chemical approach has been drawing increasing attention because of its advantage in low cost and mass production. As regards the zero-dimensional ZnO nanostructures, nanodots (NDs) or quantum dots (QDs), where the carriers are confined in all three dimensions, thus exhibiting many novel properties, by a typical solution-base method, QDs are usually directly synthesized in the solution through a ripening and precipitation process [18–20]. The problem that remains here is how to employ the low-cost chemical procedure to integrate QD arrays on some substrate. Here, by using a simple spin-coating sol–gel method with optimized sol concentration and coating times, we successfully synthesized patterned ZnO ND arrays on anodic aluminum membranes (AAMs). We have demonstrated the growth mechanism in detail, and it is believed to be a self-assembly process induced by localized negative anions in the AAM. The photoluminescence (PL) further proved that the ZnO ND arrays have excellent optical property with strong UV emission and near absence of visible emission. By varying the morphology of the AAM and adjusting the concentration of the sol, we also fabricated structures with single or several ZnO NDs isolated in the AAM nanocavities. This can be considered as a promising route to fabricate a single or coupled QD-cavity system, which is a focal point in quantum electrodynamics [21].

2. Experimental details

The AAM was synthesized in oxalic solution or phosphoric solution through a typical two-step aluminum anodic oxidation process [22, 23]. The anodic alumina membranes obtained are designated as AAM(o) and AAM(p), respectively, corresponding to oxalic and phosphoric solution. Three kinds of ethanol sol with different concentration of Zn^{2+}

[3] Author to whom any correspondence should be addressed.

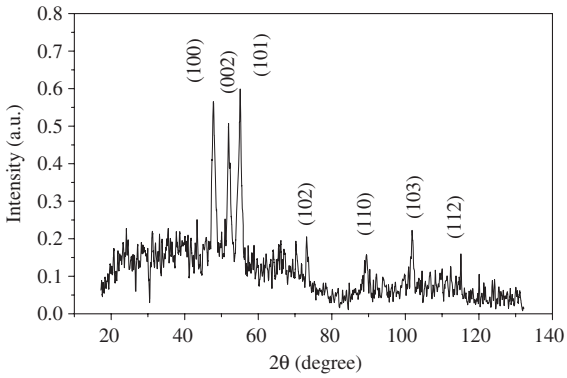

Figure 1. X-ray diffraction spectrum of ZnO products with x-ray target material: Cr ($\lambda = 2.2897$ nm).

(0.75, 0.5 and 0.25 M) were prepared using zinc acetate and monoethanolamine (MEA), while the molar ratio of the two was kept at 1. The sol was spin-coated on the AAM and preheated at 60 °C for 30 min. Then, the film was annealed at 550 °C for 3 h. Such a spin-coating and annealing process (SCAP) can be repeated twice to obtain the special nanostructure. The morphologies of the films were characterized by scanning electron microscopy (SEM; Philips XL30FEG). The crystalline structures were characterized via x-ray diffraction spectroscopy (XRD) (Bruker AXS: D8 Discover with a general area detector diffraction system using Cr as the x-ray target material, $\lambda = 2.2897$ nm). Transmission electron microscopy (TEM; JEM-2010) was also carried out. To prepare a TEM sample, small amounts of the ZnO nanofilm were taken off the AAM and put into small quantity of ethanol to form a white homogeneous suspension. Then we placed small droplets of the suspension onto a brass screen and let it dry naturally. The Raman spectra and PL measurements were carried out with Jobin-Yvon LabRAM HR 800UV micro-Raman system with a 325 nm He–Cd laser excitation, an Andor DU420 classic CCD detector and a Linkam THMS600 temperature stage.

3. Results and discussion

Figure 1 shows the XRD pattern from the ZnO products on AAM(o) obtained by using the SCAP twice with 0.5 M sol. The XRD pattern was taken from the surface of the membrane *in situ*. Seven peaks can be seen, at 48°, 52°, 56°, 73°, 90°, 101°, 114°. All of them can be indexed to the hexagonal wurtzite structure of ZnO with lattice constants $a = 0.324$ and $c = 0.520$ nm. The result proved that the obtained products are ZnO. Moreover, under the annealing temperature of 550 °C, the porous alumina membrane will remain amorphous [24]. Therefore, in the spectrum no obvious peak from γ-Al_2O_3 or α-Al_2O_3 can be detected.

Figure 2 shows the morphology of the obtained ZnO nanostructure on the AAM. A porous ZnO film grows on top of the AAM(o), as shown in figure 2(a) after one SCAP with 0.5 M sol. The ZnO film duplicated the porous alumina substrate but such a 'copy' is not a 'clone'. The surface morphology of one cell (the inset of figure 2(a)) shows that small white ZnO protuberances emerged at the vertex angle of each hexagonal cell, which suggests that the formation of the porous ZnO film on the surface of AAM(o) is not homogenous. A detailed discussion will be given later. If we further use the obtained porous ZnO film as the seed layer and repeat the same SCAP with 0.5 M ZnO sol, an interesting structure is obtained. Figure 2(b) shows the produced ZnO film, consisting of a patterned nanodot array. Some quasi-spherical particles with diameters of around 30 nm self-assemble into a flower-like morphology. Each particle on the top layer is supported by particles on the lower layer. The nanoparticles form a hierarchical dot array. We employed TEM and a selected area electron diffraction (SAED) experiment to further investigate the structures of the NDs. The results are shown in figure 2(g). We can see that the diameter of each ND is below 50 nm, which accords with the SEM results. The diffraction rings, in turn from the inside to the outside, are from (100), (002), (101), (102), (110), (103), (112) faces. All of them can be indexed to the hexagonal wurtzite structure of ZnO with lattice constants $a = 0.324$ and $c = 0.520$ nm. This is in accordance with the results from the XRD pattern.

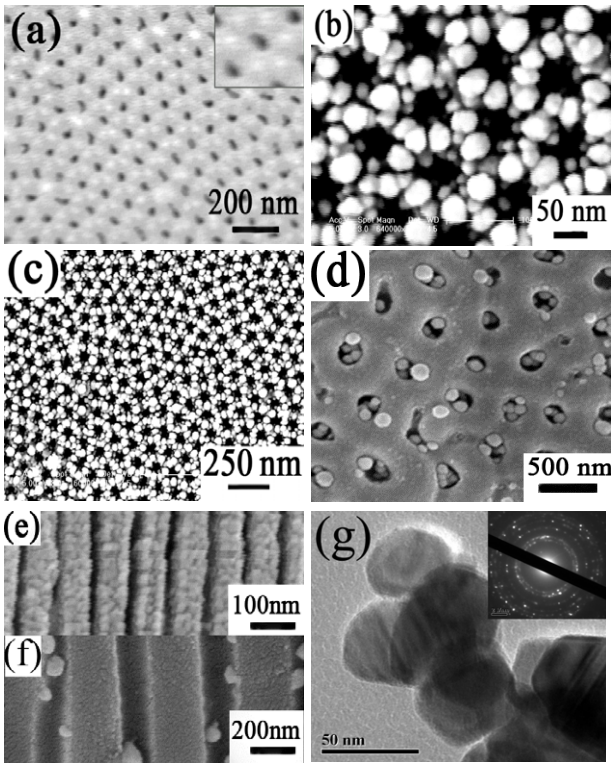

Figure 2. SEM and TEM images of ZnO nanostructures: (a) ZnO nanofilm after one SCAP with 0.5 M sol, (b) ZnO ND arrays obtained after two SCAPs with 0.5 M sol, (c) lower-magnification image proving its large-scale uniform growth, (d) ZnO nanodots grown on AAM(p) with 0.25 M sol, (e) cross-sectional images of the AAM(o) template below the ZnO nanodots (corresponding to (b) and (c)), (f) cross-sectional images of the AAM(p) template below the ZnO nanodots (corresponding to (d)), (g) TEM images of the fabricated ZnO NDs. The inset is the SAED pattern.

The possible mechanism for the formation of the interesting morphology shown in figure 2(b) may relate to the localized surface charge distribution on the surface of the AAM. It is well believed that the AAM is composed of two duplex oxide layers: an inner oxide layer which

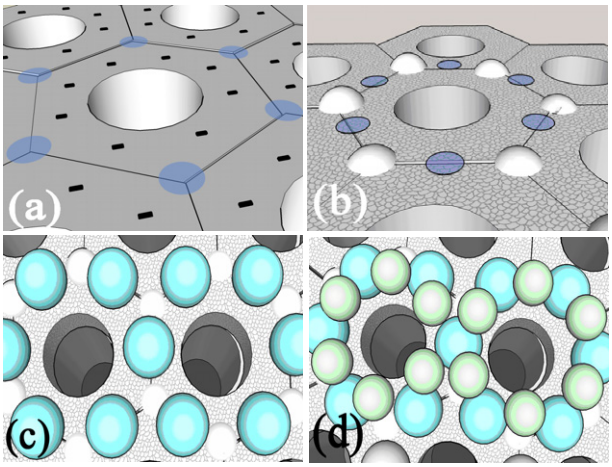

Figure 3. Schematic images of the growth of ZnO ND arrays. (a) The surface charge distribution of AAM. The '−' sign marks where the anion impurities concentrate. The round marks where ZnO grain will occur in the first SCAP. (b) The surface morphology of ZnO porous film obtained by one SCAP. The round marks where ZnO will first nucleate in the second SCAP. (c) The first layer of ZnO nanodot gradually formed. (d) After annealing, patterned ZnO nanodot arrays are finally obtained on the top of substrate.

is pure alumina, and an outer oxide layer modified with anion impurities (PO_4^{3-}, $C_2O_4^{2-}$ and OH^-), as shown in figure 3(a). Further investigation showed that the anion impurities prefer to concentrate at the intermediate part of the outer oxide layer, the outermost part of which is also scarcely anion incorporated [25, 26]. It has already been found that such localized charge distribution can affect the growth of ZnO regardless of whether it is in the pores or on the surface [26, 27]. But unlike the situation in magnetron sputtering [26], where the formation of a ZnO nanopore array is via a gradual deposition process, here in the sol–gel technique the ZnO hierarchical nanostructure is first almost simultaneously formed during the heating process. Therefore the precursor in the sol and its charge distribution also play an important role.

To assist the dissolution of zinc acetate in the ethanol, ethanolamine is added to the solution. It may act as a ligand to react with Zn^{2+} and form $Zn(H_2NCH_2CH_2OH)_2^{2+}$, which could be confirmed by the experimental phenomena that the solution became transparent immediately when ethanolamine was added. Meanwhile, the CH_3COO^- will become anions in the solution. Due to the electrostatic force, they could be attracted to the positively charged species $Zn(H_2NCH_2CH_2OH)_2^{2+}$ and surround it, thus making clusters containing zinc elements form in the solution. This is what happens when the sol is synthesized. Following the spin-coating process on the AAM, the incorporated anion impurities will impact on the clusters with negative charge outside, and the Coulomb force will move them towards to the inner oxide layer, letting the zinc species concentrate at the vertex of each hexagonal cell. Furthermore, with basic knowledge of thermodynamics it can be concluded that the smaller aperture of AAM(o) and higher viscosity of the sol give it less chance to enter the pore. This is confirmed by the cross-sectional image of the AAM(o) below the ZnO film (figure 2(e)). Meanwhile, in this condition its concentration is still not high enough to totally conceal the pore. Afterwards, during the heating process the larger ZnO grains form at the inner oxide layer (colored circle in figure 3(a)). Such preferential growth explains the small white ZnO protuberance shown at the vertex angle and the inhomogeneous porous film after annealing seen in figure 2(a). Considering the protuberance and its growing process, we believe that the charge distribution is also not uniform on this ZnO film. The protuberance surface is negatively charged, which is caused by the intrinsic dipole of ZnO. So when we repeat the above process, the next places having the lowest potential energy for the clusters containing zinc elements will be the colored circles pointed out in figure 3(b). Considering the protuberance, this time the Coulomb force will affect it in a three-dimensional way, so the exact nucleation point would be a little higher than the film surface, and the precipitated particles are prevented from inosculating together. Each point of nucleation grows bigger respectively. Moreover, while the bottom layer begins to grow, it will soon affect the charge distribution of the sol around it, so above this layer new points of nucleation occur. Finally it forms the hierarchical structure after annealing (figures 3(c) and (d)). The concentration of the precursor is also crucial to the final result. If we apply 0.25 M sol, due to the lower viscosity of the sol, after the spin process nearly nothing remains on the top surface. In contrast, if the 0.75 M sol is applied, the concentration of precursor would be just too high. Only a ZnO film with no porous structure was formed on the AAM.

The structure of single or several ZnO NDs isolated in AAM nanocavities (figure 2(d)) were obtained by using AAM(p). The sol was 0.25 M. The cross-sectional image (figure 2(f)) revealed the situation inside the channel. Also, separated ZnO NDs can be seen. The relatively large aperture and thick pore wall of AAM(p) are mostly responsible for such a result. It could be inferred that the sol first enters inside the pore of the AAM because such dilute sol cannot provide a strong enough surface tension to support itself on the top of the larger pore. Then, the spin process makes the inside sol become glued to the inner wall of the pore. During annealing, the small amount of sol soon separates to form many small droplets and they nucleate and grow separately, which finally yields such a structure. We also used 0.5 M sol on AAM(p), but only rather disordered porous film were obtained. From all the above results we can conclude that the concentration of the sol should be adjusted to properly match the morphology of the AAM to obtain valuable structures.

Resonant Raman scattering (RRS) proves to be an important tool to obtain the basic physical properties of semiconductors. Here we measure the temperature-dependent RRS of the ZnO ND arrays by using a 325 nm He–Cd laser with the back-scattering geometry. In the resonant case, the polar symmetry A_1 and E_1 modes will dominate in the spectra. From figure 4(a), we can clearly see the first-order longitudinal optic (LO) mode along with its overtones up to the third order. All modes show a red-shift and broadening behavior with increasing temperature. As is seen clearly in figure 4(c), the frequency of the 1-LO peak red-shifted from 580.1 to 575.2 cm^{-1} as the temperature increased from 83 to 368 K. The 2-LO peak behaved in the same manner. The decay and

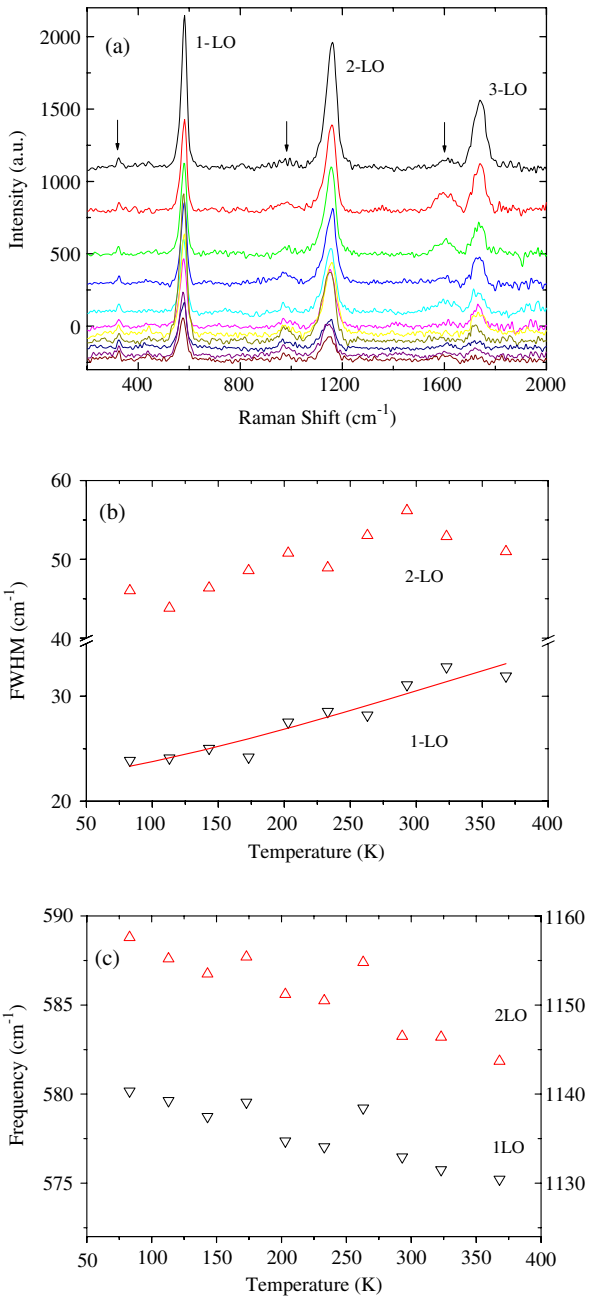

Figure 4. (a) Temperature-dependent resonant Raman spectra of ZnO ND arrays; from top to bottom the temperatures are 83 K, 113 K . . . 323 K, 368 K. (b) The FWHM of 1-LO (downward triangle) and 2-LO (upward triangle) peaks versus temperature; the solid curve is fitted with equation (1). (c) The frequency of 1-LO(downward triangle) and 2-LO (upward triangle) peaks versus temperature.

broadening of the A_1 (LO) and E_1 (LO) modes are explained by the so-called Ridley decay channel. In figure 4(b), we give the variation of the full width at half maximum (FWHM) of the 1-LO peak versus temperature and fitted with [28]

$$\Gamma(T) = \Gamma_0 + A[1 + n(\omega_1, T) + n(\omega_2, T)] \qquad (1)$$

where Γ_0 is a background contribution due to impurity or defect scattering and isotropic broadening, A is the anharmonic coefficient, $n(\omega, T)$ is the Bose–Einstein distribution function

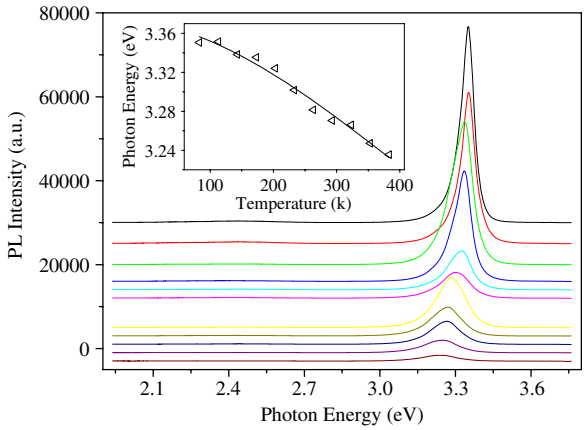

Figure 5. Temperature-dependent photoluminescence spectra of ZnO ND arrays; from top to bottom the temperatures are 83 K, 113 K . . . 383 K. The inset shows the temperature dependence of the peak energies for free-exciton emission (open triangles), together with the theoretical fit using Varshni's formula (solid curve).

and ω_1, ω_2 stand for the decay frequencies. We set $\omega_1 = 110\ \mathrm{cm}^{-1}$ and $\omega_2 = 470\ \mathrm{cm}^{-1}$. The fitting results are $\Gamma_0 = 17.2\ \mathrm{cm}^{-1}$, $A = 5.2\ \mathrm{cm}^{-1}$. The theory curve fits adequately for our 1-LO RRS peak. Apart from the three dominant peaks, the E_2(high) mode in the RRS spectra is rather weak since its scattering cross-section is close to zero. The peak around 325 cm^{-1} can be assigned to the multi-phonon process E_2(high)–E_2(low) [28]. What is interesting here is the two peaks that have emerged around 990 and 1160 cm^{-1}; they are absent in the RRS of ZnO bulk crystal [29]. We think that it is reasonable to assign them to the surface phonon (SP) modes, considering the large surface area and the small crystalline particle of the ND arrays. This can be further evidenced by the similar modes observed in other ZnO nanostructures [30, 31].

Figure 5 is the temperature-dependent PL spectra of the ZnO ND arrays. The strong UV emission can be clearly observed, while the green emission is nearly absent. Such character is maintained within the whole test range of temperature from 83 to 378 K. This suggests that the ZnO ND arrays have fewer oxygen vacancies, which are generally attributed to the origin of the green emission in ZnO [32]. This could be explained by the large surface area of ND arrays which makes ZnO NDs gain more access to the oxygen during the annealing procedure. The UV emission peak center versus temperature is fitted by Varshni's empirical formula:

$$E(T) = E(0) - \alpha T^2/(\beta + T). \qquad (2)$$

The fitting results are $E(0) = 3.368$ eV, $\alpha = 0.0006$ eV and $\beta = 312.9\ \mathrm{eV\ K}^{-1}$. The free-exciton recombination (FX) mainly contributes to near-band emission, but here $E(0)$ is 0.01 eV lower than the FX energy detected at 5 K [33]. This energy is close to that of the bond excitons, but we could not simply ascribe this emission to the recombination of bond excitons as they should vanish when the temperature is higher than 150 K [34]. This character suggests that the electronic energy distribution near the band gap must get fluctuated by some extra factors. Since we did not ever intentionally do any doping, the only thing that may reasonably explain this is that

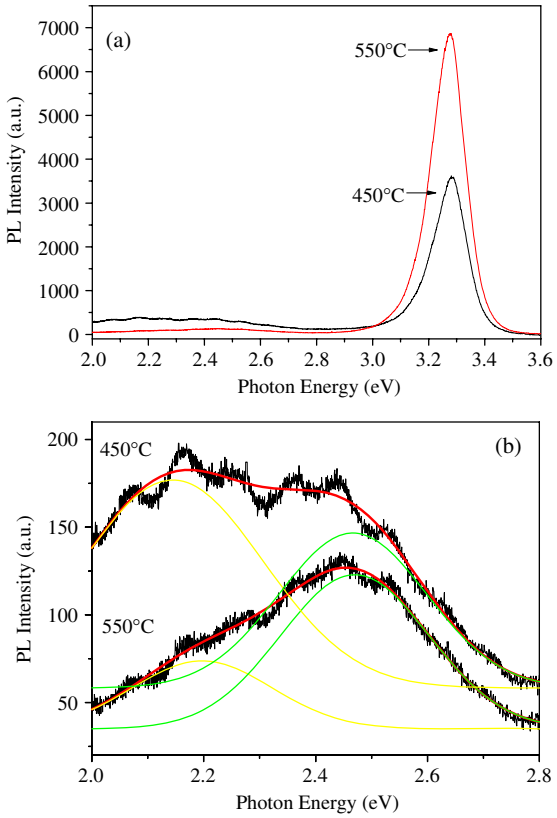

Figure 6. (a) Room-temperature photoluminescence spectra of samples annealed at different temperatures. (b) The fitting curves of the above two spectra in the visible range obtained by Gaussian fitting.

some kind of surface states occur in ZnO NDs which lower the energy gap. This could be along with the surface phonon peaks shown in the RRS spectra.

The annealing temperature also affects the photoluminescence of ZnO. We obtained the room-temperature PL spectrum for the sample annealed at 450 °C for comparison. The spin-coating process and heating rate were kept the same. From figure 6(a), we can see the defect-related visible emission is still weak. This is because the decomposition of precursors and the crystallization of ZnO in the sol–gel process already takes place at 200–300 °C [35]. 450 °C is high enough for ZnO to grow with fairly good quality. However, when annealed at 550 °C, the sample exhibited even better optical property, with much stronger UV emission and weaker visible emission. Previous researches revealed that oxygen vacancies (V_o) caused green emission centered at 2.4 eV (510 nm) [32]. But from our results (figure 6(b)), the asymmetry of both visible peaks suggest that V_o cannot be the only source. Using Gaussians, we divided them into two peaks, and found two centers around 2.2 and 2.4 eV. The former peak according to Yang *et al* can be ascribed to the interstitial oxygen (O_i), as the energy level is close to the value from theory [36, 37]. It is clear now that when the temperature is increased from 450 to 550 °C, the amount of O_i shows a significant reduction, which shows that at higher temperature the atoms have more possibility to occupy the right crystal site. Meanwhile, the intensity of emission caused by V_o did not show much change. This is believed to result from the competition of two different mechanisms. On the one hand, the number of V_o should increase as the temperature is higher and the atmosphere is not oxygen abundant [38]. On the other hand, the release of O_i makes them just compensate these vacancies. Therefore, the simultaneous work of these two effects balances the amount of V_o when the annealing temperature is raised from 450 to 550 °C.

4. Conclusions

In summary, we have presented the fabrication of patterned ZnO nanodot arrays through a spin-coating sol–gel method combined with anodic alumina membranes (AAMs). The morphology and localized negative charge surface of the AAM are crucial for the ZnO nanodots to grow in patterns. The hierarchical ZnO ND arrays with large surface area enable potential applications in sensors or detectors. The PL spectra confirmed their good emission properties. Such a structure of patterned ND arrays also exhibited special surface phonon modes in the resonant Raman scattering and near-band emission. We further fabricated structures with single or several ZnO NDs isolated in AAM nanocavities. This opens a new route to create a semiconductor QD-cavity system for potential applications in quantum information devices such as single-photon sources.

Acknowledgments

This work was supported by the Natural Science Foundation of China (50572064) and the National Minister of Education Program for Changjiang Scholars and Innovative Research Team in University (PCSIRT).

References

[1] Huang M H, Mao S, Feick H, Yan H, Wu Y, Kind H, Weber E, Russo R and Yang P 2001 *Science* **292** 1897
[2] Pearton S J, Norton D P, Ip K, Heo Y W and Steiner T 2005 *Prog. Mater. Sci.* **50** 293
[3] Law M, Greene L E, Johnson J C, Saykally R and Yang P 2005 *Nat. Mater.* **4** 455
[4] Patolsky F, Gill R, Weizmann Y, Mokari T, Banin U and Willner I 2003 *J. Am. Chem. Soc.* **125** 13918
[5] Kong X Y, Ding Y, Yang R and Wang Z L 2004 *Science* **303** 1348
[6] Pan Z W, Dai Z R and Wang Z L 2001 *Science* **291** 1947
[7] Vayssieres L 2003 *Adv. Mater.* **15** 464
[8] Tian Z R, Voigt J A, Liu J, Mckenzie B and Mcdermott M J 2002 *J. Am. Chem. Soc.* **124** 12954
[9] Tian Z R, Voigt J A, Liu J, Mckenzie B, Mcdermott M J, Rodrigues M A, Konoshi H and Xu H 2003 *Nat. Mater.* **2** 821
[10] Li C, Fang G, Su F, Li G, Wu X and Zhao X 2006 *Nanotechnology* **17** 3740
[11] Zheng M J, Zhang L D, Li G H and Shen W Z 2002 *Chem. Phys. Lett.* **363** 123
[12] Cheng H M, Lin K F, Hsu H S, Lin C J, Lin L J and Hsieh W F 2005 *J. Phys. Chem.* B **109** 18385
[13] Xu W L, Zheng M J, Ding G Q and Shen W Z 2005 *Chem. Phys. Lett.* **411** 37
[14] Andelman T, Gong Y, Polking M, Yin M, Kuskovsky I, Neumark G and O'Brien S 2005 *J. Phys. Chem.* B **109** 14314
[15] Li F, Ding Y, Gao P, Xin X and Wang Z L 2004 *Angew. Chem. Int. Edn* **43** 5238
[16] He F Q and Zhao Y P 2006 *Appl. Phys. Lett.* **88** 193113
[17] Zhang Z *et al* 2007 *Appl. Phys. Lett.* **90** 153116

[18] Noack V and Eychmüller A 2002 *Chem. Mater.* **14** 1411
[19] Cheng H M, Lin K F, Hsu H C and Hsieh W F 2006 *Appl. Phys. Lett.* **88** 261909
[20] Guo L, Yang S, Yang C, Yu P, Wang J, Ge W and Wong G K L 2000 *Appl. Phys. Lett.* **76** 2901
[21] Badolato A, Hennessy K, Atatüre M, Dreiser J, Hu E, Petroff P M and Imamoğlu A 2005 *Science* **308** 1158
[22] Masuda H and Fukuda K 1995 *Science* **268** 1466
[23] Li Y B, Zheng M J, Ma L and Shen W Z 2006 *Nanotechnology* **17** 5101
[24] Xu W L, Zheng M J, Wu S and Shen W Z 2004 *Appl. Phys. Lett.* **85** 4364
[25] Choi J, Luo Y, Wehrspohn R B, Hillebrand R, Schilling J and Gösele U 2003 *J. Appl. Phys.* **94** 4757
[26] Ding G Q, Shen W Z, Zheng M J and Fan D H 2006 *Appl. Phys. Lett.* **88** 103106
[27] Wu G S, Xie T, Yuan X Y, Li Y, Yang L, Xiao Y H and Zhang L D 2006 *Solid State Commun.* **134** 485
[28] Cuscó R, Alarcón-Lladó E, Ibáñez J, Artús L, Jiménez J, Wang B and Callahan M J 2007 *Phys. Rev.* B **75** 165202
[29] Scott J F 1970 *Phys. Rev.* B **2** 1209
[30] Chen S J, Liu Y C, Jiang H, Lu Y M, Zhang J Y, Shen D Z and Fan X W 2005 *J. Cryst. Growth* **285** 24
[31] Ursaki V V, Tiginyanu I M, Zalamai V V, Rusu E V, Emelchenko G A, Masalov V M and Samarov E N 2004 *Phys. Rev.* B **70** 155204
[32] Vanheusden K, Warren W L, Seager C H, Tallant D R, Voigt J A and Gnade B E 1996 *J. Appl. Phys.* **79** 7983
[33] Tsukazaki A, Ohtomo A, Yoshida S, Kawasaki M, Chia C H, Makino T, Segawa Y, Koida T, Chichibu S F and Koinuma H 2003 *Appl. Phys. Lett.* **83** 2784
[34] Zhang Y, Lin B X, Sun X K and Fu Z X 2005 *Appl. Phys. Lett.* **86** 131910
[35] Ohyama M, Kozuka H and Yoko T 1997 *Thin Solid Films* **306** 78
[36] Yang Y, Yan H, Fu Z, Yang B, Xia L, Xu Y, Zuo J and Li F 2006 *Solid State Commun.* **138** 521
[37] Lin B X, Fu Z X and Jia Y B 2001 *Appl. Phys. Lett.* **79** 943
[38] Wu X L, Siu G G, Fu C L and Ong H C 2001 *Appl. Phys. Lett.* **78** 2285